iScience

CellPress
OPEN ACCESS

Article

LET-Dependent Low Dose and Synergistic Inhibition of Human Angiogenesis by Charged Particles: Validation of miRNAs that Drive Inhibition

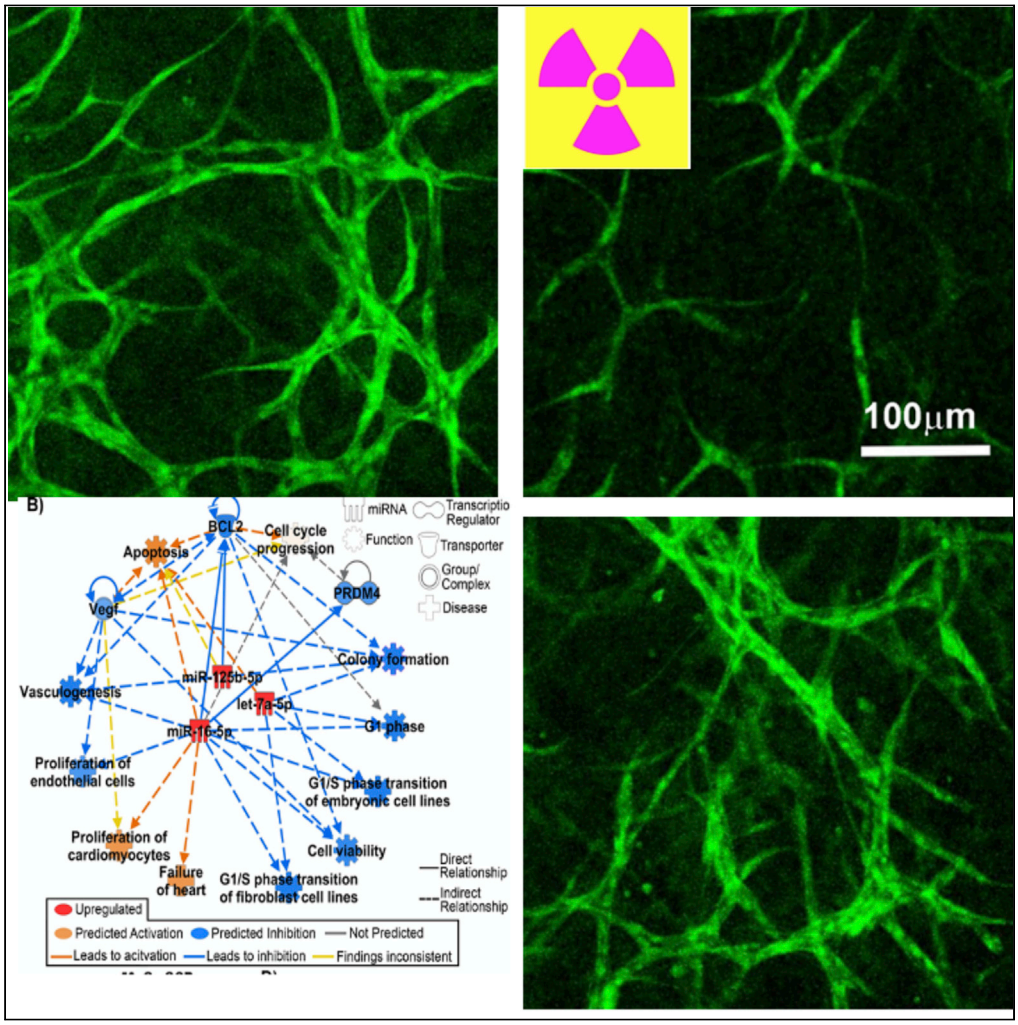

Yen-Ruh Wuu, Burong Hu, Hazeem Okunola, ..., Margareth Cheng-Campbell, Afshin Beheshti, Peter Grabham

afshin.beheshti@nasa.gov (A.B.)
pwg2@columbia.edu (P.G.)

HIGHLIGHTS

Space radiation inhibits angiogenesis synergistically at low doses by 2 mechanisms

Candidates for bystander transmission are microRNAs

Three previously identified miRNAs showed downregulation of their angiogenesis targets

Synthetic miRNA inhibitors were used to reverse the inhibition of angiogenesis

Wuu et al., iScience *23*, 101771
December 18, 2020
https://doi.org/10.1016/j.isci.2020.101771

iScience

CellPress
OPEN ACCESS

Article

LET-Dependent Low Dose and Synergistic Inhibition of Human Angiogenesis by Charged Particles: Validation of miRNAs that Drive Inhibition

Yen-Ruh Wuu,[1] Burong Hu,[2] Hazeem Okunola,[3] Amber M. Paul,[4,5] Elizabeth A. Blaber,[5,6] Margareth Cheng-Campbell,[5,6] Afshin Beheshti,[7,*] and Peter Grabham[3,8,*]

SUMMARY

Space radiation inhibits angiogenesis by two mechanisms depending on the linear energy transfer (LET). Using human 3D micro-vessel models, blockage of the early motile stage of angiogenesis was determined to occur after exposure to low LET ions (<3 KeV/AMU), whereas inhibition of the later stages occurs after exposure to high LET ions (>8 KeV/AMU). Strikingly, the combined effect is synergistic, detectible as low as 0.06 Gy making mixed ion space radiation more potent. Candidates for bystander transmission are microRNAs (miRNAs), and analysis on miRNA-seq data from irradiated mice shows that angiogenesis would in theory be downregulated. Further analysis of three previously identified miRNAs showed downregulation of their targets associated with angiogenesis and confirmed their involvement in angiogenesis pathways and increased health risks associated with cardiovascular disease. Finally, synthetic molecules (antagomirs) designed to inhibit the predicted miRNAs were successfully used to reverse the inhibition of angiogenesis.

INTRODUCTION

Travel in space involves exposure to microgravity and space radiation not normally found on earth (Simonsen et al., 2020). Charged particles in space are composed of protons and heavier charged ion particles (HZE ions). HZE particles are the high-energy component of galactic cosmic radiation (GCR) and are generally more effective than terrestrial X-rays or γ-rays in inducing biological damage (Durante and Cucinotta, 2011). Furthermore, they are considered to present a high mortality risk for astronauts (Cucinotta et al., 2017).

Ion particles penetrate matter in a straight track structure and deposit energy per unit of track length, defined as the linear energy transfer (LET). They also produce secondary irradiations. It can be thought of as a measure of the average thickness of the track with respect to energy deposition. Space radiation consists of ions with a range of LETs. Low LET particles include high-energy protons, whereas high LET particles include ions such as silicon, iron, and oxygen. In general, higher LET ions are more biologically effective than low LET ions, although this is not the case for the inhibition of angiogenesis as addressed in this study. By and large, astronauts on missions in a low Earth orbit (LEO) are exposed to lower dose rates of HZE particles and more protons, whereas crews from missions beyond LEO experience a higher flux of HZE particles and higher dose rates. Together with microgravity, charged particles present risks for the cardiovascular system (Hughson et al., 2018) and data from Apollo lunar astronauts suggest possible deep space radiation effects on the vascular endothelium and the cardiovascular system (Delp et al., 2016), although more data are required for confirmation (Cucinotta et al., 2016).

The radiation element of the effect of the space environment on the cardiovascular system has been investigated by simulating space radiation on Earth using specific HZE ions or protons at facilities such as the National Aeronautics and Space Administration (NASA) Space Radiation Laboratory (NSRL) at Brookhaven National Laboratory (BNL). Experiments using animals, human cells, and tissues show a number of harmful effects (Boerma et al., 2015; Mitchell et al., 2019). The human vascular system comprises the heart, arteries, veins, and small vessels including the smallest – and most abundant – capillaries. With a combined length of tens of thousands of miles, the capillaries are a major target for charged particles. In fact, a single particle will traverse a large number of capillaries depending on the trajectory of the ion and the density of

[1]Drexel University College of Medicine, Philadelphia, PA 19129, USA

[2]Department of Radiation Medicine, School of Public Health and Management, Wenzhou Medical University, Wenzhou, Zhejiang 325035, China

[3]Center for Radiological Research, Department of Radiation Oncology, College of Physicians and Surgeons, Columbia University, VC 11-243, 630 West 168th Street, New York, NY 10032, USA

[4]Universities Space Research Association, Columbia, MD 21046, USA

[5]Space Biosciences Division, NASA Ames Research Center, Moffett Field, CA 94035, USA

[6]Department of Bioengineering, Center for Biotechnology & InterdisciplinaryStudies, Rensselaer Polytechnic Institute, Troy, NY 12180, USA

[7]KBR, Space Biosciences Division, NASA Ames Research Center, Moffett Field, CA 94035, USA

[8]Lead Contact

*Correspondence: afshin.beheshti@nasa.gov (A.B.), pwg2@columbia.edu (P.G.)

https://doi.org/10.1016/j.isci.2020.101771

capillaries in the target tissue or organ, making them a major target for radiation. Ground-based studies have shown that endothelial cells and small blood vessels (micro-vessels *in vitro* and capillaries *in vivo*) are especially sensitive to space radiation. Endothelial cells show pro-atherosclerotic transcriptomic and proteomic responses in response to ^{56}Fe ions (Baselet et al., 2017) and the inhibition of pro-angiogenic genes in response to protons (Girdhani et al., 2012). *In vivo* mouse retinal endothelium shows oxidative damage and apoptosis after exposure to oxygen ions (Mao et al., 2018). Furthermore, there is a loss of hippocampal microvasculature after exposure to ^{56}Fe ions (Mao et al., 2010). Other studies have shown that *in vitro* and *in vivo* models exposed to proton and HZE radiation increase DNA oxidation, myocardial fibrosis, and endothelial dysfunction (Soucy et al., 2011; Yu et al., 2011). Thus, there is a wide range of responses of blood vessels to space radiation. In previous studies on the human 3D micro-vessel models, we have shown several effects of charged particles contributing to the dysfunction of micro-vessels. DNA damage by heavy ions is prolonged (Grabham et al., 2012), endothelial barrier function is disrupted (Sharma et al., 2013), and mature vessel morphology is damaged by charged particles (Grabham et al., 2011). Most relevant to the present study, angiogenesis is inhibited by charged particles (Grabham et al., 2011); moreover, this inhibition is due to two distinct mechanisms depending on the LET of the ions. First, protons inhibit the early motile stage of angiogenesis, and second, ^{56}Fe ions inhibit the later stages of tubulogenesis (Grabham and Sharma, 2013; Grabham et al., 2013).

Thus, there are a variety of responses of blood vessels to simulated space radiation, and the pathways involved are complex with multiple signaling pathways involved. For example, there are multiple signals activated by molecules triggered by oxidative stress and also multiple signals activated by DNA damage. This complexity presents a challenge to understanding the underlying mechanisms that control the response of micro-vessels to space radiation. One approach to understanding this complexity is to identify master regulatory molecules, and we have recently confirmed the identification of specific microRNAs (miRNAs) as a means to identify these master regulatory molecules (Beheshti et al., 2018; Malkani et al., 2020).

miRNAs are short (~22 nucleotide long) sequences of non-coding RNA that can regulate gene expression at the transcriptional and translational level and interact directly with proteins (Vanderburg and Beheshti, 2020b). miRNAs have recently been implicated as predictors and regulators for several diseases, including cancer (Macfarlane and Murphy, 2010), neurodegenerative diseases (Konovalova et al., 2019), and autoimmune disorders (Chen et al., 2016). miRNAs have also been found to be involved in biological responses to ionizing radiation (Simone et al., 2009). Therefore, our research is focused on identifying individual miRNAs or their networks that are likely to play a major role in regulating the angiogenic response(s) to space radiation-associated stressors. Ultimately, miRNAs could also be targeted for biomarker and countermeasure development. We have previously identified and validated a spaceflight signature of circulating miRNAs associated with cardiovascular damage (Beheshti et al., 2018, 2019; Malkani et al., 2020). We have also shown that these circulating miRNAs can be systemic drivers in the host to promote increased health risks due to heavy and light ion exposure (Malkani et al., 2020; Paul et al., 2020). Lastly, we have shown the highly conserved nature of these miRNAs across different species from rodents to humans (Malkani et al., 2020). From this previous work, the miRNAs that we discovered to be associated with space-radiation-related cardiovascular health risks are specifically miR-16-5p, miR-125b-5p, and let-7a-5p. These three miRNAs have also been heavily implicated in the clinic to be associated with heart disease, cardiovascular disease, and inhibition of angiogenesis (Condorelli et al., 2010).

Here, we have focused on the inhibition of angiogenesis by space radiation. First, we elucidated the precise LETs that inhibit angiogenesis by each of the two mechanisms, the inhibition of motile tip activity and the later inhibition of tubulogenesis. Second, the effect of the mixed LETs, as in space, were shown to be synergistic. Third, global miRNA analysis in mice exposed to simulated Galactic Cosmic Radiation (GCR) irradiation of mixed ions for significantly disrupted regulated pathways associated with micro-vessel function focusing on angiogenesis, cell cycle, apoptosis, and microtubule regulation pathways. Further analysis was conducted on three miRNAs that were previously identified as part of a larger spaceflight-associated circulating miRNA signature for increased health risk (Malkani et al., 2020). These three miRNAs were determined to regulate angiogenesis and are key regulators determined from both the global analysis conducted in the present study and previous work (Malkani et al., 2020). We predicted that these three miRNAs have a direct effect on the inhibition of angiogenesis. Lastly, we inhibited these miRNAs *in vivo* using antagomirs to verify our predicted protection of angiogenesis following space-like radiation. These data prove that the complex inhibition of angiogenesis caused by simulated space radiation is mediated through specific miRNAs and these effects can be reversed using antagomirs.

RESULTS

We have previously shown that protons and ^{56}Fe ions both inhibit angiogenesis in human 3-D micro-vessel models. Human umbilical vein cell (HUVEC) irradiations are carried out 24 hr after seeding when the cells have just begun to extend motile tips and are mostly not connected up to each other yet. Micro-vessels are then measured after 7 days culture (Grabham et al., 2011). Full inhibition was achieved at 0.8 Gy for both charged particles (1 GeV protons and 1 GeV ^{56}Fe ions). Although this was considered a relatively low dose at the time, it is now known that a combination of large error margins in the assay and the lack of information on doses below 0.2 and 0.4 Gy underestimated the biological effect of the radiation and that the effective doses are in fact much lower (see below). Nevertheless, the result was sufficient to reveal an unexpected similar relative biological effectiveness (RBE) for protons and ^{56}Fe ions. Further studies showed that the heavy and light ions inhibit angiogenesis by distinct mechanisms (Grabham and Sharma, 2013). Light ions inhibit the early stages of angiogenesis when motile tip cells sprout out into the matrix. Heavy ions inhibit the later stages of angiogenesis (tubulogenesis), when the new pioneer endothelial cell processes widen to form tubes. Furthermore, the addition of the protein kinase C (PKC) stimulator phorbol ester, phorbol-12-myristate-13-acetate (PMA), was able to reverse the effect of protons but not ^{56}Fe ions. Protein kinase C isomers of different types are known to be second messengers involved in angiogenesis. The angiogenic factors – vascular endothelial growth factor receptors – act as a docking site for phospholipase C-gamma which in turn activates PKC (Patel-Hett and D'Amore, 2011). Also, studies have implicated PKC in vessel formation and the effects of radiation (Girdhani et al., 2013; Willey et al., 2010). Although the use of PMA here does not give much new information on the role of specific PKCs in vasculogenesis, it has proved useful for distinguishing between inhibition of the early stages by low LET ions and the later stages by high LET ions.

Angiogenesis Is Inhibited by Charged Particles with Different LETs

With energies at 1 GeV/n for each of protons and ^{56}Fe ions from previous studies (Grabham et al., 2013), the LET values for each of these particles are at the extreme ends of the spectrum of the charged particles experienced in space. However, there are several species of charged particles found in space, and they are present in different quantities. To assess the risk factors of all radiations, it is necessary to determine the LET range of each type of inhibition of angiogenesis. For example, in the case of low LET ions, solar particle events contain protons of several energies, and the potency of all is needed for calculations of risk. Similarly, there are several high LET ions in GCR in addition to ^{56}Fe ions, and the effectiveness of all is needed to determine if they can act collectively. A number of different ion species and energies were tested to determine the range of each effect using a dose of 0.75 Gy. It can be seen from Figure 1A that all ion species and energies tested inhibited the formation of micro-vessels (morphology shown in Figure 3). However, addition of PMA 15 min prior to irradiation restored micro-vessel growth in a subset of charged particle treatments. Protons at energies of 1 GeV/n and 200 MeV/n and helium ions at energies of 1 GeV/n and 125 MeV/n showed a rescue of the phenotype with PMA treatment, whereas the heavier ions – carbon, oxygen, silicon and ^{56}Fe ions – did not. When these data are plotted as a logarithmic LET plot (Figure 1B), it can be seen that charged particles with an LET of 3 KeV/AMU and below inhibited angiogenesis in a way that can be reversed by the action of PMA. Conversely, particles with an LET of 8 KeV/AMU or more inhibit angiogenesis in a way that cannot be reversed by the action of PMA.

Motile Tip Activity Is Inhibited by Charged Particles with Different LETs

The effective LET ranges that affect motile tip activity should match the effective LET ranges for the two types of inhibition of micro-vessel formation in Figure 1. Early motile tip activity is known to be inhibited by 1 GeV/n protons, whereas 1 GeV/n ^{56}Fe ions do not. One-day-old micro-vessel cultures were fixed 2 hr after irradiation with the same dose (0.75 Gy), range of particles and energies used in Figure 1, then immunostained for microtubules, which are characteristically tightly bundled in active motile tips (Grabham et al., 2013). Moreover, the addition of PMA is known to rescue the motile tip phenotype (Grabham et al., 2013). The counts of motile tips per cell are shown in Figure 2. Protons at energies of 1 GeV/n and 200 MeV/n and helium ions at energies of 1 GeV/n and 125 MeV/n inhibited motile tip activity by approximately 80%. Furthermore, the phenotype is rescued by the addition of PMA, as in the final micro-vessel phenotype seen in Figure 1. The heavier ions – carbon, oxygen, silicon, and ^{56}Fe ions – did not affect motile tip activity (Figure 2A). When these data are plotted as a logarithmic LET plot (Figure 2B), it can be seen that charged particles with an LET of 3 KeV/AMU and below inhibit motile tip activity in a way that can be reversed by the action of PMA. Conversely, particles with an LET of 8 KeV/AMU or more do not inhibit motile tip activity and are not rescued by PMA. These LET limits are complimentary to the limits seen for micro-vessel formation.

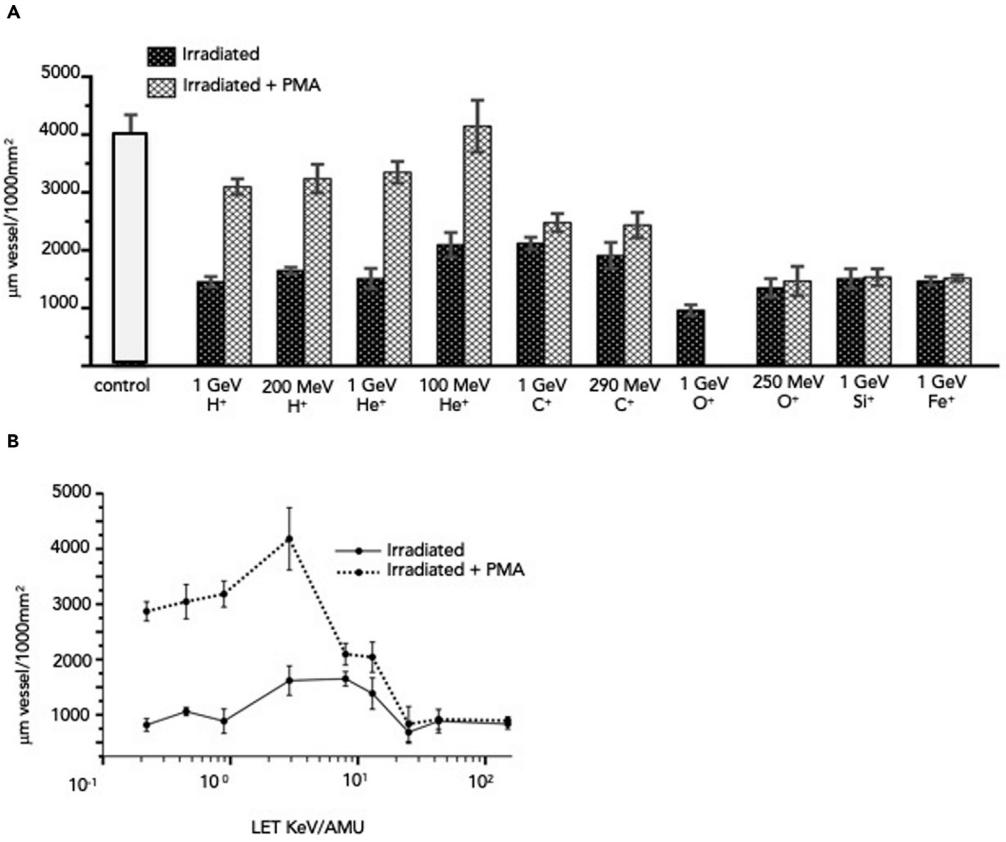

Figure 1. Inhibition of Micro-vessel Development by a Range of Charged Particles and Energies

Early developing micro-vessel cultures were exposed to 0.75 Gy of each charged particle and allowed to develop over the next 6 days. Micro-vessels were then fixed stained, and micro-vessel length was determined (Transparent Methods).

(A) Average length of micro-vessels per unit area. Cultures without PMA exhibit inhibition of micro-vessel formation after exposure to all ion species and energies. When PMA is added to the cultures, the phenotype after exposure to protons (1 GeV/n and 200 MeV/n) and helium ions (1 GeV/n and 125 MeV/n) is rescued and micro-vessels are formed. For heavier ions – C, O, Si, and ^{56}Fe – PMA does not rescue the phenotype, and micro-vessel formation remains inhibited.

(B) Logarithmic LET plot of the data in (A). Inhibition of micro-vessel formation after exposure to charged particles with an LET of 3 KeV/AMU or lower is rescued by PMA. Charged particles with an LET of 8 KeV/AMU or higher remain inhibited in the presence of PMA. Data are represented as mean ± SEM.

History of Micro-vessel Growth

Although the morphology of inhibited micro-vessels suggests that the early stages of angiogenesis are inhibited by light ions and the later stages of tubulogenesis are inhibited by heavy ions, there are other possibilities. In both cases, the micro-vessels could have formed fully and then either pruned back (light ions) or collapsed (heavy ions). To resolve this question, the history of micro-vessel growth is shown by visualization of the vessels and the collagen tunnels they secrete. Since collagen is deposited by the cells to form tunnels only when the micro-vessels are mature, it can be used to determine at what stage the charged particles affect angiogenesis. Figure 3 shows the micro-vessel structures and collagen deposits after exposure to high and low LET charged particles at a dose of 0.2 Gy. Control cultures (Figure 3A) have mostly wide vessels with robust collagen tunnels, indicating that endothelial cells have completed all stages of development. Figure 3B shows the effect of ^{56}Fe ions. The thin processes have little collagen deposits confirming that the early stage of pioneer tunnel formation has occurred followed by a cessation of development before micro-vessel widening and collagen deposition. Proton effects are shown in Figure 3C. Most structures are wide but short, and collagen deposition is robust. This indicates that motile tip activity and pioneer tunnel formation was inhibited, although the later stages of tubulogenesis and collagen deposition in the truncated structures still occurred. Exposure to a mixture of each charged particle results in a diverse phenotype representing both light and heavy ions.

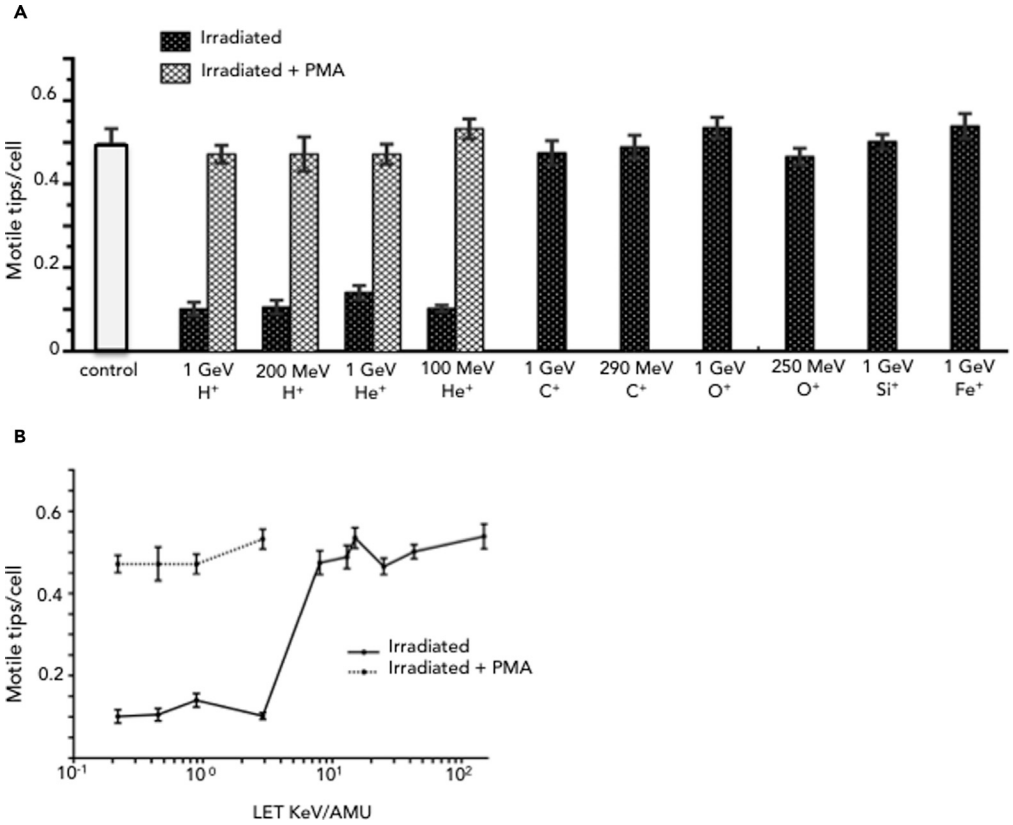

Figure 2. Inhibition of Motile Tip Activity by a Range of Charged Particles and Energies

Early developing micro-vessel cultures were exposed to 0.75 Gy of each ion particle and fixed 2 hr later followed by immunostaining for tubulin to determine the number of motile tips per cell (Transparent Methods). Low LET but not high LET charged particles cause a significant reduction in the number of motile tips per cell. Phorbol ester added to cultures before exposure to low LET ions restores the motile tip activity. .Data are represented as mean ± SEM.

(B) Logarithmic LET plot of the data in (A). Inhibition of motile tip activity occurs after exposure to charged particles with an LET of 3 KeV/n or lower and the phenotype can be rescued by PMA. Charged particles with an LET of 8 KeV/n or higher do not affect motile tip activity. Data are represented as mean ± SEM.

Mixed Particle Effects – Protons and ^{56}Fe Ions

The finding that thin vessels are incompletely developed prompted us to adopt a more concise angiogenesis assay. Thin processes were eliminated by only scoring wider vessels along with some other refinements (Transparent Methods). Since the charged particles in space are a mixture of various heavy and light ions, the combined effect is of interest, especially since light and heavy ions inhibit angiogenesis by distinct mechanisms and therefore may have complex effects on the final micro-vessel growth. Initial experiments using lower doses of mixed ions than previously used, in anticipation of additive effects, revealed that the micro-vessel assay was not sensitive enough. Lower doses of individual ions appeared to be effective, and the error margins in the original assay were high (Grabham et al., 2011). Previously, the lowest doses investigated were 0.2 Gy and 0.4 Gy of protons and ^{56}Fe ions, respectively, so the effects of even lower doses were unknown. The assay of final micro-vessel formation was therefore improved to resolve the precise doses that inhibit angiogenesis (see Transparent Methods). Initial experiments to investigate mixed particle effects were carried out with a 1:1 mixture of 1 GeV/n protons and 1 GeV/n ^{56}Fe ions. Controls included a parallel dose response for each individual ion exposed at the same time as mixed particles. Both individual ions inhibited micro-vessel formation at lower doses than previously detected (Figure 4). Of note is that, the RBEs are still similar for each ion, and the dose at which the reduced micro-vessel formation is significant is 0.125 Gy (proton P = < 0.03, ^{56}Fe ions P = < 0.02). A 1:1 mixture of ions with the same total dose inhibited micro-vessel growth extremely effectively. Therefore, mixed ions were much more potent than the same total dose of each ion individually making the response synergistic rather than simply additive. A log plot shows more clearly at which doses the response is noteworthy (Figure 4B). A mixed ion exposure

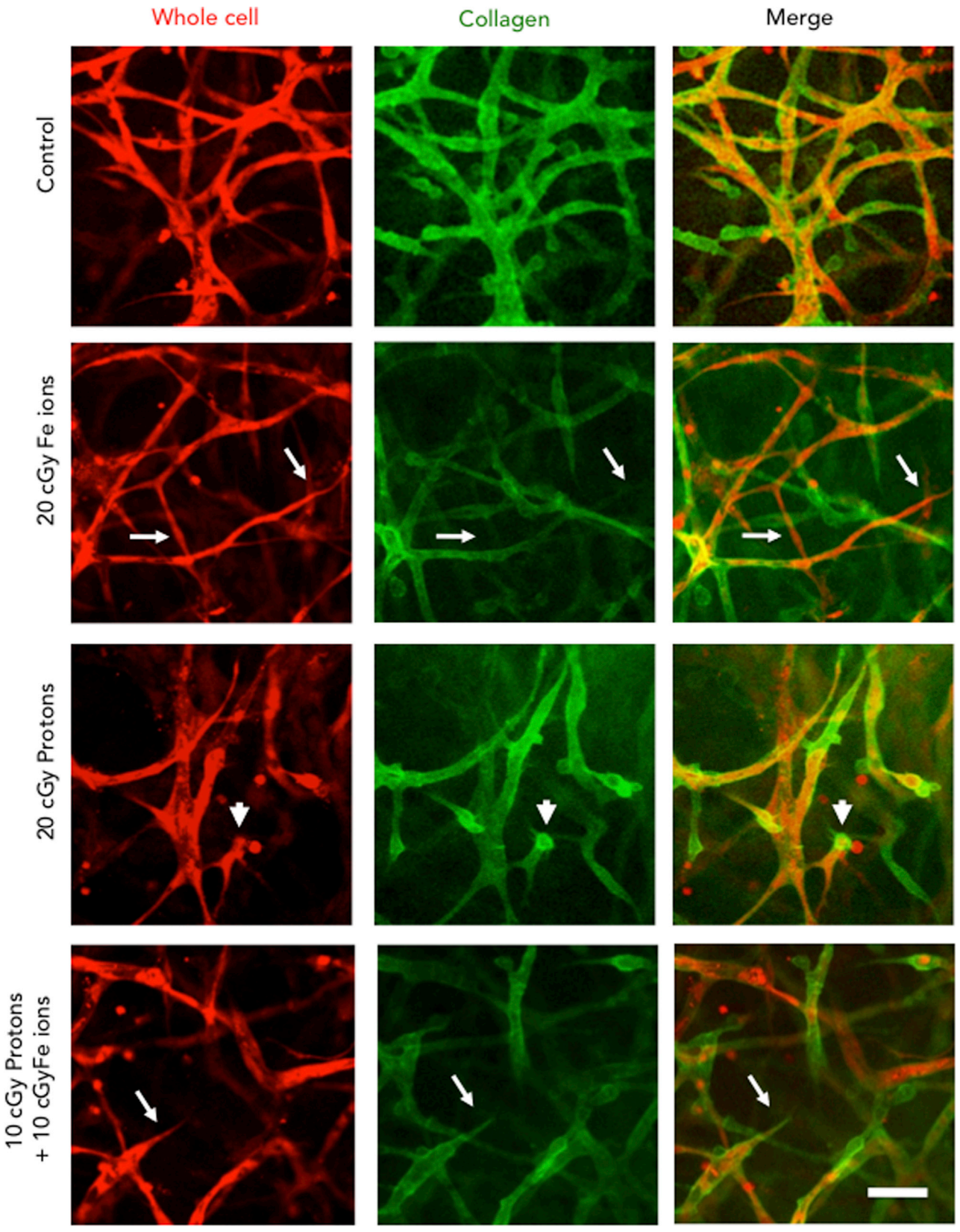
Whole cell
Collagen
Merge
Control
20 cGy Fe ions
20 cGy Protons
10 cGy Protons
+ 10 cGyFe ions

Figure 3a. History of Micro-vessel Growth

One-day-old cultures were exposed to a dose of 0.2 Gy ^{56}Fe ions (1 GeV/n), 0.2 Gy protons (1 GeV/n), and a 1:1 mixture of 0.1 Gy ^{56}Fe ions (1 GeV/n) and 0.1 Gy protons (1 GeV/n). Six days after irradiation, the mature cultures were stained for micro-vessels (red) and immunostained for collagen (green).
Unirradiated controls have mostly wide vessels with extensive collagen tunnels surrounding them(9as shown
Cultures exposed to ^{56}Fe ions are predominantly thin with very little collagen deposition (arrows).
Cultures exposed to protons are wide but short and stunted but with substantial collagen around the short micro-vessels (arrowhead).
Exposure to a mixture of each charged particle results in a diverse phenotype. There are pioneer structures (arrow) and widened vessels (arrowhead) albeit with a pointed end. Bar represents 50 μm.

causes inhibition significantly at a total dose of 0.03 Gy, that is, 0.015 Gy of each ion (P = < 0.05), more than four times more effective than the individual ions alone. Alternative X axes show the estimated fluence for each ion. ^{56}Fe ions at 0.03 Gy have a fluence of 10 cell hits per 1000 cells, whereas protons at 0.03 Gy have fluence of 8 hits per cell. The morphology of micro-vessels grown after exposure to mixed ions is shown in Figure 1. Mixtures of abnormal morphologies are evident such as thin micro-vessels and abrupt terminations to micro-vessels.

Mixed Particle Effects – He Ions and Si Ions

To confirm the synergistic inhibition of micro-vessel formation by a mixture of heavy and light ions, the effect of another pair of ions was tested. From the LET range studies, it is predicted that any light ion with at least an LET of 3 KeV/AMU together with any heavy ion LET of at least 8 KeV/AMU would combine to produce a synergistic effect. The resulting combined effect of 1 GeV/n He ions and 600 MeV/n Si ions proved this to be the case (Figure 5). In this assay, the effective He ion dose was similar to that of protons (significant at 0.125 Gy, P = < 0.001), and the effective Si ion dose was slightly higher than that of ^{56}Fe ions (0.25 Gy, P = < 0.002). The combined significant dose was also slightly higher than that of the mixture of protons and ^{56}Fe ions (0.06 Gy, P = < 0.0001); although the synergistic effect is quite clear, 0.06 Gy of each ion produces a response that is more than twice that of He ions and four times that of Si ions. The morphology of micro-vessels that developed after a mixture of 0.06 Gy He ions and 0.06 Gy Si ions shows a profound inhibition of angiogenesis (Figure 5B). Thus, the synergistic response is likely relevant to any mixture of charged particles from each category of heavy and light ions.

Identification of miRNA as Potential Angiogenesis Regulators

The synergistic effect of heavy and light ions together is a highly complex response that requires control by key regulators. We have previously identified and validated a spaceflight signature of circulating miRNAs associated with cardiovascular damage (Beheshti et al., 2018, 2019; Malkani et al., 2020). We have also shown that these circulating miRNAs can be systemic drivers in the host to promote increased health risks due to heavy and light ion exposure (Malkani et al., 2020; Paul et al., 2020). Lastly, we have shown the highly conserved nature of these miRNAs across different species from rodents to humans (Malkani et al., 2020). To expand on the humanized 3D microvasculature tissue model to the impact of space radiation exposure to the full organism, we utilized tissues from female C57BL/6 mice (n = 10) that were exposed to a 0.5 Gy acute dose of the simplified GCR simulation (SimGCRSim) (Simonsen et al., 2020). SimGCRSim consists of 5 ions: protons at 1000MeV/n, ^{28}Si at 600 MeV/n, ^{4}He at 250 MeV/n, ^{16}O at 350 MeV/n, ^{56}Fe at 600 MeV/n, and protons at 250 MeV/n. This mixture and dose contain elements of heavy and light ions at doses sufficient to induce each of the individual types of angiogenesis inhibition and the synergistic effect described above. We also chose female mice due to the relevance of NASA proposing that the first person to step on Mars should be a female (Condorelli et al., 2010). The mice were euthanized 24 hr after irradiation (Paul et al., 2020). Unirradiated sham female C57BL/6 mice were also used as controls. Plasma and heart tissues from these mice were used for miRNA sequencing (see Methods) to capture the potential cardiovascular impact of GCR exposure in the host.

To understand the global impact of miRNAs on the micro-vessels and the cardiovascular system after GCR exposure, we first performed global miRNA-seq analysis to determine the overall profile of the miRNAs in the tissues (Figures 6A and 6B). The overall pattern of the miRNAs reveals distinct global miRNA differences between the tissues. Interestingly, the plasma shows less distinct separation between the irradiations on the global scale as compared to the heart tissue (Figure 6B). GCRsim in the heart produced a significantly different miRNA profile when compared to the sham and gamma-irradiated mice, as seen by the t-Distributed Stochastic Neighbor Embedding (t-SNE) plot in Figure 6B. To find which miRNAs are systemically being regulated due to GCRsim irradiation, we determined differentially expressed overlapping miRNAs between both the plasma and the heart comparisons between GCRsim vs Sham-irradiated mice. From this

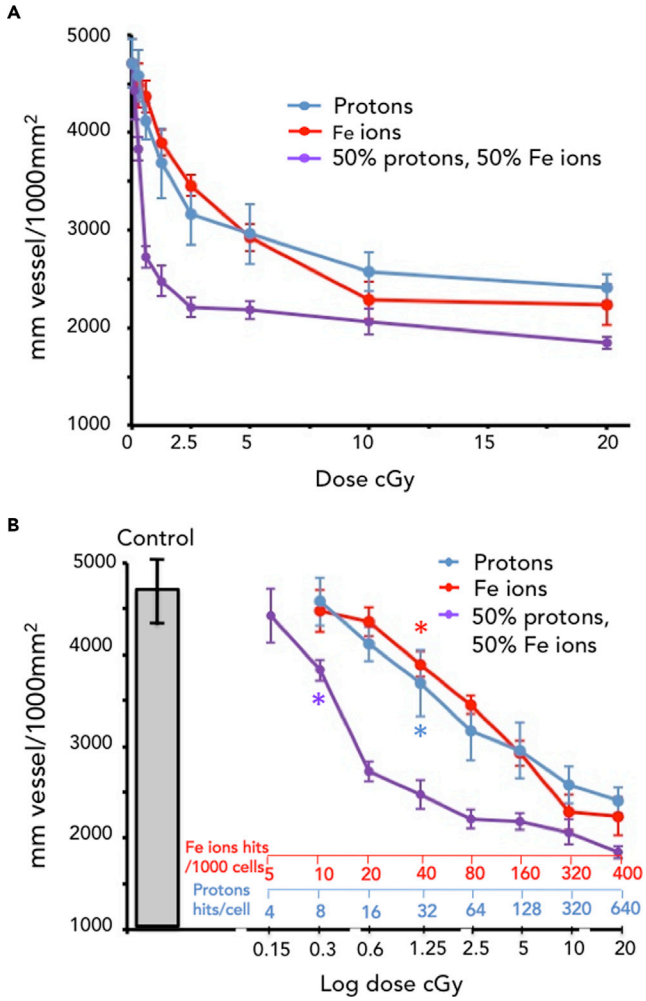

Figure 4. Dose Response for the Inhibition of Angiogenesis by Individual and Mixed Charged Particles (Protons and ^{56}Fe Ions)

Early developing cultures (one day after seeding into matrices) were exposed to either protons (1 GeV/n) or ^{56}Fe ions (1 GeV/n) or a 1:1 mixture of each ion (protons delivered first). At maturity, six days after exposure, micro-vessel cultures were fixed, stained, and analyzed.

(A) Linear plot of total mature vessel length per 1000 μm^2 area. Individual ions each inhibit the formation of micro-vessels by 1500 μm at a dose of 0.05 Gy. A total dose equivalent of equal proportions of mixed ions inhibits the formation of micro-vessels by around 2000 μm at a dose of 0.06 Gy.

(B) Logarithmic dose plot of the graph in (A). Individual protons and ^{56}Fe ions show a similar dose response whereby the reduction of micro-vessel length is reduced significantly at a dose of 0.125 Gy (blue and red asterisks, protons $p < 0.03$, ^{56}Fe ions $p < 0.02$, respectively). Total dose equivalent of mixed ions has a more than additive effect becoming statistically significant at a dose of 0.03 Gy (purple asterisks, $p < 0.05$). Alternative x axis scales show the fluence per cell for protons (blue) and for fluence per 1000 cells for ^{56}Fe ions (red). Data are represented as mean ± SEM.

analysis, we determined 19 miRNAs that are overlapping (Figure 6C). When comparing to the differentially expressed miRNAs to gamma- vs sham-irradiated mice, no overlap of miRNAs was determined. This indicates that there is a distinct miRNA profile for GCR irradiation.

In a companion paper by (Malkani et al., 2020), we have determined a universal circulating miRNA signature associated with spaceflight. We wanted to determine the overlap of this miRNA signature with the GCRsim response. The miRNAs involved with this signature are being expressed with the majority being upregulated in the heart tissue (Figure 6D). Two of the miRNAs (miR-146a-5p and miR-223-3p) overlap with the overlapping systemic miRNAs in our analysis. Additionally, we have displayed the rest of the 19 systemic miRNAs in the same heatmap (Figure 6D). When observing if these miRNAs will impact cardiovascular

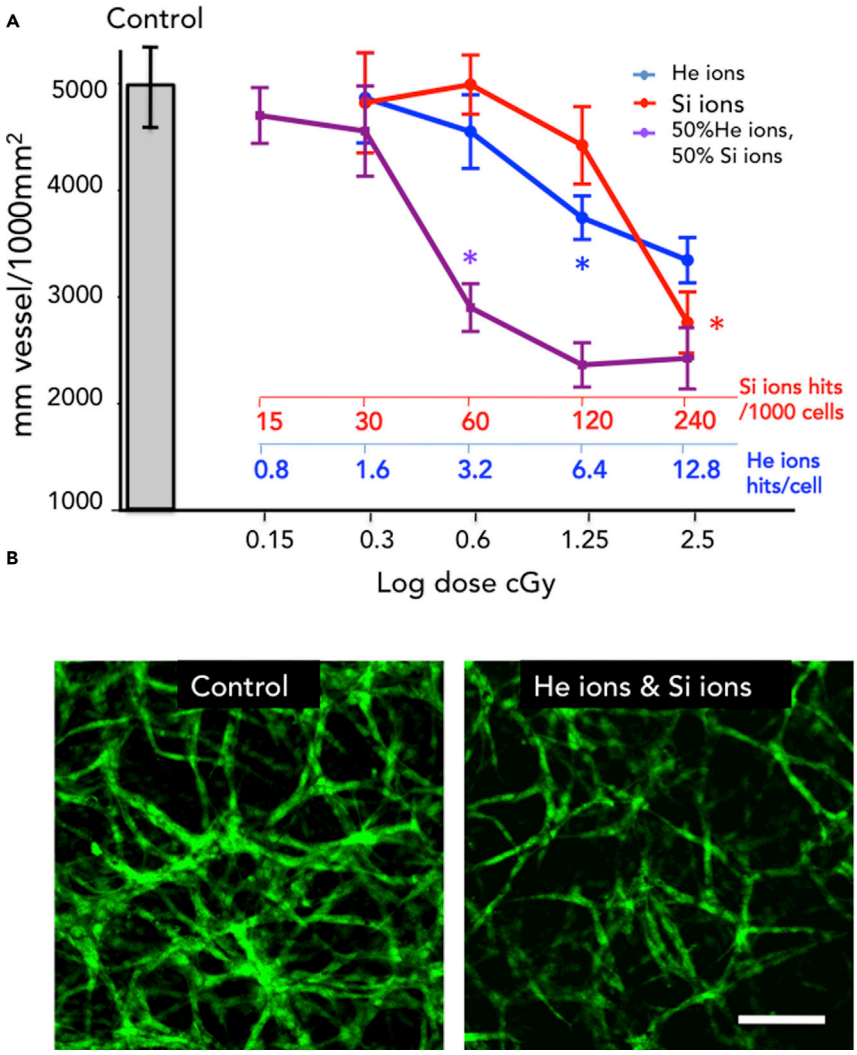

Figure 5. Dose Response for the Inhibition of Angiogenesis by Individual and Mixed Charged Particles (He Ions and Si Ions)

Developing cultures were exposed to either He ions (1 GeV/n) or Si ions (600 MeV/n) or a 1:1 mixture of each ion (helium ions delivered first).

(A) Logarithmic dose plot of total mature vessel length per 1000 μm^2 area. Individual Helium ions and Si ions show dose responses whereby the reduction of micro-vessel length is reduced significantly at a dose of 0.125 Gy helium ions (blue asterisk, p = < 0.001) and 0.25 Gy Si ions (red asterisk p = < 0.002). Total dose equivalent of mixed ions has a more than additive effect becoming statistically significant at a dose of 0.06 Gy (purple asterisks, $p < 0.05$). Alternative x axis scales show the fluence per cell for helium ions (blue) and for fluence per 1000 cells for Si ions (red). Data are represented as mean ± SEM.

(B) Morphologies of control and mixed ions (total dose 0.125 Gy) from the experiment in 5A. Fluorescently stained for all proteins with 5-(4,6-dichlorotriazinyl) aminofluorescein, (5-DTAF). Mixed ion exposure greatly inhibits micro-vessel formation. Bar represents 100 μm.

function, we find surprising overlap to what is observed in the clinic. A review of miRNAs in heart disease by (Condorelli et al., 2010) described in detail miRNAs that are involved with heart failure and cardiovascular disease. The 19 miRNAs all appear as key players with cardiovascular disease. For example, the observed downregulation of miR-1 in the heart for GCRsim irradiated mice vs sham mice is associated with heart failure and heart disease. The other miRNAs are associated with similar cardiovascular phenotypes.

Next, we determined the significantly regulated pathways of interest including angiogenic, cell cycle, apoptosis, and microtubule pathways (Figure 6E). From the subset of significant miRNAs (p value < 0.05)

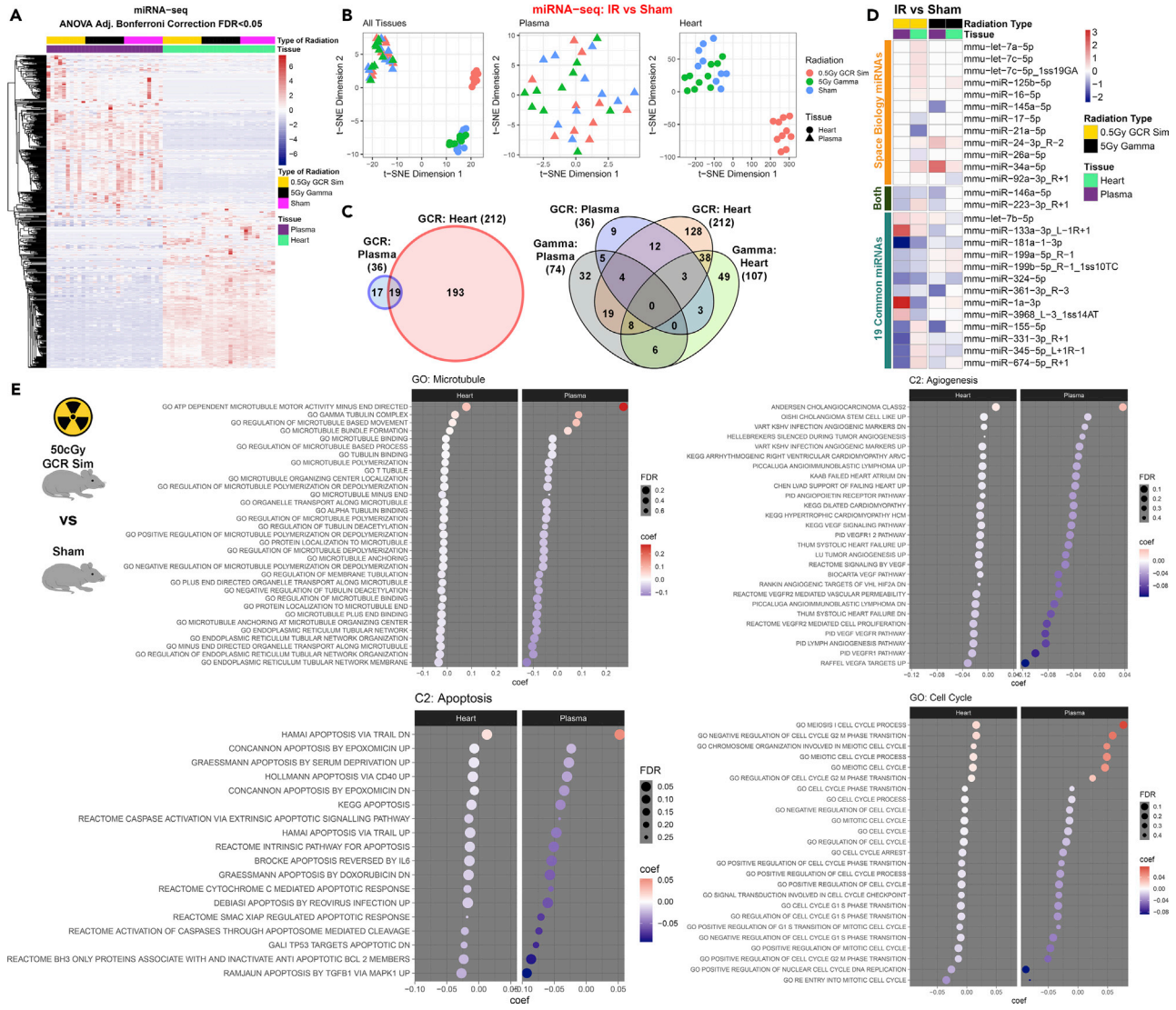

Figure 6. MicroRNA-Sequencing on Mice Irradiated with GCRSim Demonstrating miRNA Involvement with Angiogenesis during Space Radiation

(A) Global miRNA differences occurring in plasma and heart tissue from mice irradiated with GCRsim. Heatmap representation of miRNA-sequence data for the significantly regulated genes with False Discovery Rate (FDR) <0.05 analyzed by analysis of variance (ANOVA) across the samples.

(B) Combined and individual t-SNE plots for significantly expressed miRNAs for plasma and heart tissue.

(C) Venn diagram of the significantly regulated miRNAs between the different experimental conditions.

(D) miRNA fold changes between irradiated (IR) conditions vs sham groups for each GCRsim and gamma. miRNAs from our proposed spaceflight signature are included, as well as the additional common miRNAs for GCRsim between the plasma and heart tissues implicated by miRNA-seq in (C).

(E) Gene ontology (GO) and canonical pathway (C2) analysis on miRNA-seq data from GCR irradiation. Pathway analysis for GO and C2 terms (from MSigDB) with an FDR <0.25 cutoff was considered significant. Specific pathways related to microtubules, angiogenesis, apoptosis, and cell cycle were selected and plotted. The coef term represents coefficient determined from the RBiomirGS R package for miRNA pathway analysis. This term, if positive, will indicate an upregulation for the pathway and if negative a downregulation for the pathway based on the miRNA analysis. Specific significantly regulated pathways for angiogenesis, microtubules, cell cycle, and apoptosis were utilized for this analysis. The dot plots are color coded for shades of blue for the degree of downregulation and shades of red for the degree of upregulation. Also, the size of the dots represents the FDR significance, with the larger the dot, the more significant.

See also Tables S1 and S2.

(Tables S1 and S2), we were able to determine significantly regulated pathways from the miRNA gene targets. Angiogenic factors and microtubule regulatory factors (motility) were screened for insights into the effects on angiogenesis. While cell cycle factors and apoptosis factors were screened as known radioresponse controls, as expected, the majority of the cell cycle factors are also shown to be downregulated,

except for meiotic cell cycle pathways. It has previously been shown that radiation damage could potentially activate meiosis-specific pathways and genes after mitotic catastrophe induced by radiation exposure (Ianzini et al., 2009). Additionally, we do not see increases in apoptosis potentially because the cells are postmitotic and resistant to these doses used in this study (Grabham et al., 2011). Lastly, miRNA response in the plasma shows stronger response than in the heart tissue supporting the view that the response is systemic.

Inhibition of miRNAs to Counter the Effects of Space Radiation

We have previously identified and validated a spaceflight signature of three specific miRNAs associated with cardiovascular damage: these are let-7a-5p, miR-125b-5p, and miR-16-5p (Beheshti et al., 2018, 2019; Malkani et al., 2020). We found that these miRNAs were upregulated in mature micro-vessels and validated as effectors of simGCRsim-induced micro-vessel collapse (Malkani et al., 2020). From global miRNA-seq analysis on the plasma and heart tissues from irradiated mice, we determined the significantly associated pathways for miRNA gene targets being impacted by GCR irradiation in the tissues (Figure 7A). From this analysis, the gene targets for all 3 miRNAs were present and were shown to be downregulated. Since it is known that miRNAs will downregulate or silence the majority of the gene targets when upregulated, this analysis is in perfect alignment with what we expect should occur after GCR exposure to the tissues.

Furthermore, additional pathway analysis was conducted utilizing ingenuity pathway analysis to predict specific functions, diseases, and genes that will be impacted by the upregulation of the three miRNAs (Figure 7B). We find that the direct effect of these three miRNAs show inhibition of angiogenesis and cell cycle functions with increased activity of apoptosis (Figure 7B). In addition, we observed increased health risks associated with cardiovascular disease.

The three miRNAs (miR-125, miR-16, and let-7a) were inhibited by using antagomirs (Krutzfeldt et al., 2005). Antagomirs were applied collectively at a concentration of 0.5 μm 24 hr before irradiation and on days 1 and 2 during micro-vessel development. Morphology of the developed micro-vessels was assessed 7 days after irradiation with 0.5 Gy SimGCRSim. We observed irradiation-mediated inhibition of angiogenesis since the micro-vessels had failed to develop. Furthermore, this impact of SimGCRSim exposure was reversed by application of the three antagomirs. Thus, angiogenesis was protected by inhibiting the miRNAs, proving that the impairments caused by simulated deep space radiation are at least partially mediated through miRNAs and can be reduced using antagomirs (Figures 7C and 7D). Further experiments were carried out to confirm the micro-vessel promoting effect of the inhibition of miRNAs with antagomirs. In this case, the micro-vessels were grown in nutrient-depleted medium (50% normal micro-vessel growth medium and 50% EBM-2 media without additives). Antagomirs were applied on days 0, 1, and 2 during micro-vessel development. All antagomirs significantly restored full micro-vessel growth over the growth-depleted controls (Figure S1).

DISCUSSION

In summary, we have delineated the types of ion species and LET ranges for the inhibition of micro-vessel development for each mechanism of the inhibition of angiogenesis. The low doses required for these effects have been more accurately defined here and are significantly lower than previously thought for each type of inhibition (Grabham et al., 2011). Importantly, we have also shown that when developing micro-vessels are exposed to a combination of heavy and light ions, there is a synergistic effect that is detectible at an even lower dose. To our knowledge, this is the first example of synergy and additionally the lowest dose effect seen on a human tissue in response to space radiation. This is a novel finding since it illustrates that space radiation can collectively affect an important biological process and thus greatly increase the effective dose over single ions. This makes the lower doses found in space more of a potential threat to astronaut health. The low doses indicate transmission via a bystander response, potentially mediated through miRNAs. Analysis of miRNA-seq data from the serum of irradiated mice demonstrate that pathways associated with angiogenesis would in theory be downregulated. Furthermore, analysis of the miRNA in micro-vessels exposed to GCR showed a significant association with the gene targets of angiogenic pathways for miRNA gene targets. Three previously identified miRNAs (miR-125, miR-16, and let-7a) were all involved, and ingenuity pathway analysis showed that these miRNAs would indeed lead to the inhibition of proteins in pathways leading to angiogenesis. These analyses were then substantiated by

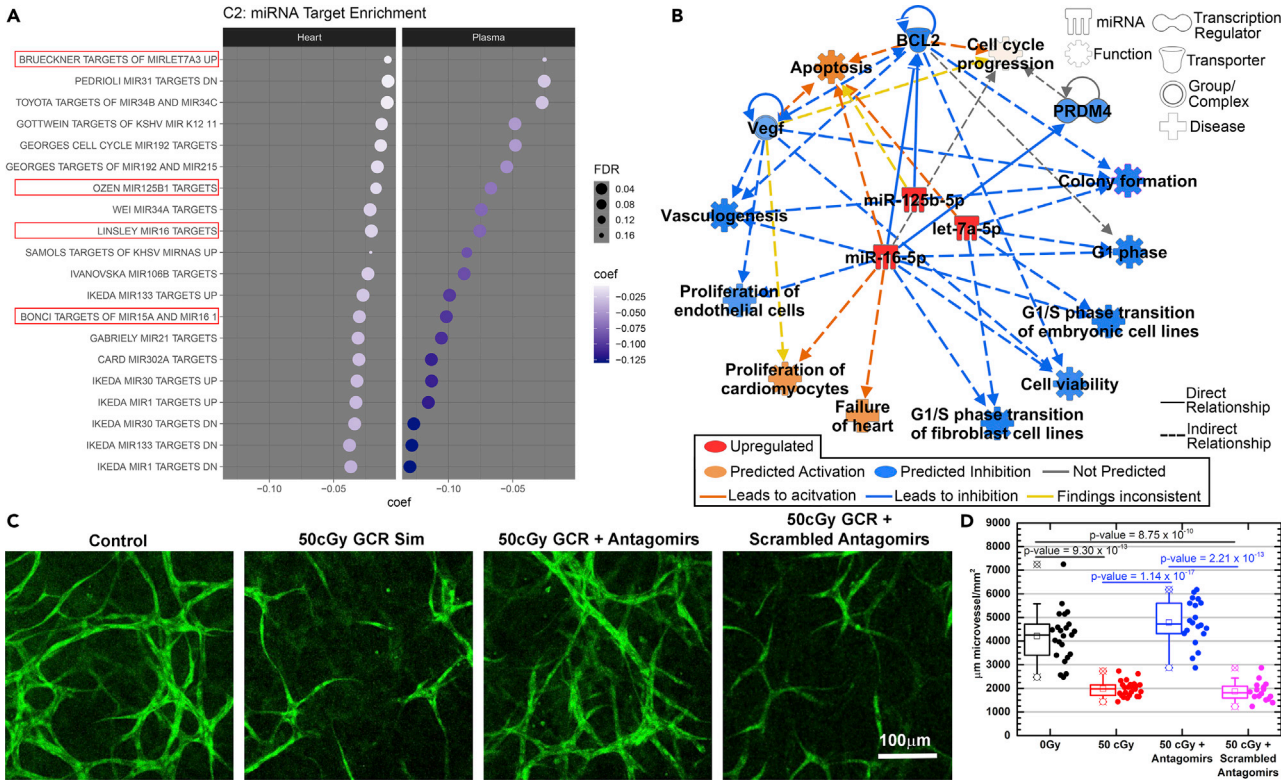

Figure 7. Inhibition of Key miRNAs Prevent GCR Damage on Micro-vessels

(A) Pathway analysis for the C2 terms related to miRNA enriched targets with an FDR <0.25 cutoff. The coef term represents coefficient determined from the RBiomirGS R package for miRNA pathway analysis. This term if positive will indicate an upregulation for the pathway and if negative a downregulation for the pathway based on the miRNA analysis. Specific significantly regulated pathways for angiogenesis, microtubules, cell cycle, and apoptosis were utilized for this analysis. The dot plots are color coded for shades of blue for the degree of downregulation and shades of red for the degree of upregulation. Also, the size of the dots represents the FDR significance, with the larger the dot, the more significant. The pathways related to miR-16-5p, let-7a-5p, and miR-125b-5p are outlined with red.

(B) Pathway analysis for miR-16-5p, let-7a-5p, and miR-125b-5p utilizing ingenuity pathway analysis (IPA). Specific angiogenic, cell cycle, and apoptotic factors were shown.

(C and D) Reversal of GCRsim effects in micro-vessels. C. micro-vessel morphology in controls, irradiated, and irradiated with antagomirs and scrambled antagomirs. HUVECs were seeded into the gel matrix and irradiated with 0.5 Gy simGCRsim 24 hr later. Antagomirs (0.5 μm each) were added to cultures at 48 and 72 hr. After full formation of micro-vessels (a total of 7 days culture), micro-vessels were fixed and stained for all proteins with 5-(4,6-dichlorotriazinyl) aminofluorescein (DTAF). D. Analysis of micro-vessels shows that antagomirs have restored the inhibition of angiogenesis by simGCRsim, whereas scrambled antagomirs have not. Data are represented as mean ± SEM.

See also Figure S1.

inhibiting the miRNAs using antagomirs and showing that angiogenesis in 3D micro-vessel models was restored after exposure to mixed GCR radiation.

The growth and formation of blood micro-vessels is a complex, multi-stage process, and there are many stages at which charged particles with different physical properties can affect angiogenesis. Therefore, it is not surprising that charged particles with very different physical properties can inhibit angiogenesis by different mechanisms. Using two assays, one for total micro-vessel formation and one for early motile tip activity, and using a number of different species of charged particles with different energies, we demonstrated that the inhibition of micro-vessel formation is demarcated into two groups for this endpoint. Light ions (protons and He ions) with an LET of 3 keV/AMU or lower inhibited the early motile stages of micro-vessel formation, whereas heavy ions of 8 keV/AMU or higher (carbon, oxygen, silicon, and iron ions) prevented the later stages of development. Thus, the response to charged particles is separated into two types according to the ion species and LET. Since the radiation in space is a mixture of heavy and light ions, there is the potential for both types of inhibition to occur and possibly have combined effects (see

below). These results also have relevance to cancer radiotherapy by charged particles. Carbon ion therapy would fall into the heavy ion group while proton and He ion therapy would fall into the light ion group. Both would be advantageous in inhibiting tumor vasculature compared to gamma rays, which are known to promote tumor vessel growth (Sofia Vala et al., 2010; Wild-Bode et al., 2001). Not all biological responses to charged particles are grouped in this way, illustrating that there are a wide variety of biological responses to charged particle radiation. For example, heavy ion radiation-induced intestinal and colon tumorigenesis has a peak RBE at a particular LET of 69 keV/AMU (Suman et al., 2016) and the highest activation of the nuclear factor kβ pathway in kidney cells by heavy ion beams has an optimal range of 91–272 keV/AMU (Hellweg et al., 2011).

What are the potential consequences of the inhibition of angiogenesis for astronaut health? The most apparent is rarefaction – the gradual loss of micro-vessels because of the lack of replacement of damaged vasculature by angiogenesis. This eventually leads to a decrease in the number of perfused capillaries in tissues and several resulting pathologies. Cancer therapies that target angiogenesis by inhibiting vascular endothelial growth factor (VEGF) signaling illustrate the clinical problems that can occur after rarefaction. Angiogenesis inhibitors cause pain in the extremities, high blood pressure, a long-term increase in the risk of hypertension, arterial thromboembolism, cardiac ischemia, and cardiac dysfunction (Abdel-Qadir et al., 2017; Goligorsky, 2010; Moslehi, 2016). The magnitude of the effect of charged particles depends on the amount of angiogenesis occurring in the body. Therefore, at any time, micro-vessel regeneration would only be occurring in a very small subset of the microvasculature according to what damage had previously occurred. This is especially true as in space the microgravity environment reduces kinetic damage and abrasion to the body, thus reducing damage and the need for micro-vessel regeneration. However, there are indications that microvascular damage and the following regeneration is still occurring in space. Firstly, although physical wear and tear to the body might be reduced in the microgravity environment, astronauts still experience small injuries during space flight (Scheuring et al., 2009), in addition to a constant low level of micro-vessel turnover without visible injury. Secondly, other factors in the space environment such as altered oxygen concentration, heavy ion effects on mature micro-vessels (Grabham et al., 2011, 2013), and microgravity could also compound the damage to micro-vessels and create a greater requirement for angiogenesis. Even so, rarefaction is a relatively slow process, but it is incremental and accumulative, and as such, the length of time exposed to space radiation is an important factor for consideration. Long space missions such as those to Mars would induce rarefaction over a relatively long period producing a more severe loss of micro-vessels.

Alterations in the secretion of bioactive materials from the irradiated endothelial cells are another important potential cardiovascular health consequence of the inhibition of angiogenesis by space radiation. During angiogenesis, there are a range of molecules secreted and actively involved in the process, and their actions are not always confined to angiogenesis since they often have other functions. Furthermore, some angiogenesis signals are shared with stress response signals. Exposure to radiation is known to produce the free radical – nitrous oxide (NO) (Clarencon et al., 1999), and NO is also an angiogenic factor in addition to being a vasodilator (Ziche and Morbidelli, 2000). Another secreted angiogenic factor, VEGF, was found to be downregulated in endothelial cells after exposure to protons (Girdhani et al., 2012). Inhibition of VEGF activity is known to induce cardiovascular damage via redox-sensitive processes (Neves et al., 2018).

The low doses required for inhibition indicate a bystander response, especially in the case of heavy ions that are effective at fluences much lower than one traversal per cell (Figures 4 and 5). Thus, bioactive materials, such as secreted proteins, miRNAs, and exosomes (containing proteins and nucleic acids), are likely to be released by targeted cells and affect other cells and tissues. Since we have previously shown and validated a spaceflight signature of circulating miRNAs associated with cardiovascular damage (Beheshti et al., 2018, 2019; Malkani et al., 2020), miRNAs are a prime focus here. Furthermore, these circulating miRNAs can be systemic drivers in the host to promote increased health risks due to heavy and light ion exposure (Malkani et al., 2020; Paul et al., 2020) and are conserved across different species from rodents to humans (Malkani et al., 2020). In addition, miRNAs are known to regulate and influence entire pathways associated with spaceflight health risk (Vanderburg and Beheshti, 2020b). In particular, the three candidate miRNAs circulating in the blood stream of exposed mice were predicted and then validated in the same micro-vessel models at the mature stage of development (Malkani et al., 2020). In accordance with this hypothesis, we utilized here the same miRNAs and model during the earlier stages of development

(angiogenesis) that produced similar beneficial results for inhibiting space radiation impact. This underscores that these miRNAs are master regulators that can control multiple responses to space radiation. In support, there are overlaps in the three miRNAs with those seen in earlier studies of fibroblasts and leukocytes exposed to the space environment (Hughes-Fulford et al., 2015; Zhang et al., 2016) and in ground-based space radiation experiments with mice (Templin et al., 2012). In general, miRNAs are known to play a role in cardiovascular disease (Colpaert and Calore, 2019). Interestingly, the three miRNAs, miR-16-5p, miR-125b-5p, and let-7a-5p, are known to be involved in various aspects of cardiovascular disease. For example, it has been shown that miR-125b-5p and miR-16-5p are included in some of the most abundant miRNAs in the pericardial fluid that was identified to be associated with cardiovascular disease (Kuosmanen et al., 2015). All three miRNAs have been shown to be involved with ischemic stroke, which is closely related to microvascular and blood vessel dysfunction (Eyileten et al., 2018). Interestingly, during development, miR-16a-5p and miR-125b-5p have also been shown to be related to onset of cardiovascular and cerebrovascular disease if upregulated in the placental tissues (Hromadnikova et al., 2015). Our studies with the 3D human developing micro-vessel models are also in agreement with these results since this model can represent development of the vasculature. From our results, space radiation is inducing these miRNAs to be upregulated, thus downregulating the target proteins, which is in turn associated with increased risk of cardiovascular disease and other vascular type diseases according to the literature. This concept is proven here by the inhibition of miRNAs and the resulting restoration of angiogenesis. With the simple application of the antagomirs as a countermeasure to block the increase of these miRNAs, we have, for the first time, shown an amelioration of the complex response(s) of angiogenesis to space radiation. Therefore, the ability of miRNAs to be potential master regulators is underscored by the fact that two types of the inhibition of angiogenesis in addition to nutrient deprivation are reversed by inhibiting the miRNAs.

With the simple application of the antagomirs as a countermeasure to block the increase of these miRNAs, we have for the first time shown an amelioration of the complex response(s) of angiogenesis to space radiation. This opens a new avenue of possible mitigative strategies based on the regulation and understanding of master regulators. The implications of these results not only have impact with space radiation research but also provide clues of possible therapeutics for terrestrial diseases in the clinical setting. As indicated by our results and the current knowledge in the literature, future studies are warranted to apply similar methods in for clinical associated diseases.

Limitations of the Study

A major limitation to the study is that the methodology of miRNA pathway analysis is still a relatively new field that is not yet widely accepted, and the proof of concept is still in its infancy. However, previous recent publications by the corresponding authors do support the authenticity of the miRNA analysis and in particular the success of using antagomirs (in this paper and in the associated Cell Press paper [Malkani et al., 2020]) to verify the miRNA predictions in the human micro-vessel models. Other major limitations stem from the availability of the kind of radiation used in the study. There is only one facility that can produce the heavy ions utilized for such experimentation – the BNL in Long Island, NY, and beam time is limited to several hours per annum. Furthermore, the mixed radiation representing that in space is only been in operation for the last year or so. This inhibits rapid ad hoc studies to expand the findings. For example, the three miRNAs focused on here were studied collectively when an examination of each individually would be highly desired. Such studies are, however, underway and planned for the future.

Resource Availability

Lead Contact

Further information and requests for resources and reagents should be directed to, and will be fulfilled by, the Lead Contact, Peter Grabham (pwg2@cumc.columbia.edu).

Materials Availability

This study did not generate any unique reagents.

Data and Code Availability

The miRNA-seq raw fastq files can be found on NASA's GeneLab data repository/platform (https://genelab.nasa.gov/). The accession number for the heart tissues miRNA-seq reported in this paper

is in GeneLab: GLDS-334, DOI: 10.26030/cg2g-as49; and the accession number for the plasma miRNA-seq reported in this paper is in GeneLab: GLDS-336, DOI: 10.26030/qasa-rr29.

METHODS

All methods can be found in the accompanying Transparent Methods supplemental file.

SUPPLEMENTAL INFORMATION

Supplemental Information can be found online at https://doi.org/10.1016/j.isci.2020.101771.

ACKNOWLEDGMENTS

We would like to thank Drs. Peter Guida, Adam Rusek, Michael Sivertz, and the NSRL team at BNL for their assistance and expertise with irradiation studies. This work was supported by NASA grants; NNX11AR03G, and NNX14AR22G awarded to P.G and the Translational Research Institute for Space Health through NASA Cooperative Agreement NNX16AO69A (T-0404) awarded to A.B.

AUTHOR CONTRIBUTIONS

The corresponding authors are P.G. and A.B. The paper is divided into two main interdisciplinary sections: micro-vessel studies by P.G. and miRNA analysis by A.B., with joint studies by both.

Conceptualization, P.G. and A.B.; Methodology, A.B. and P.G.; Formal Analysis, A.B. and P.G.; Investigation, all authors; Resources, all authors.; Writing – Original Draft, A.B. and P.G.; Writing – Review & Editing, all authors; Visualization, P.G. and A.B.; Supervision, P.G. and A.B.; Funding Acquisition, P.G. and A.B.

DECLARATION OF INTERESTS

The authors declare no competing interests.

Received: July 18, 2020
Revised: October 19, 2020
Accepted: October 31, 2020
Published: November 25, 2020

REFERENCES

Abdel-Qadir, H., Ethier, J.L., Lee, D.S., Thavendiranathan, P., and Amir, E. (2017). Cardiovascular toxicity of angiogenesis inhibitors in treatment of malignancy: a systematic review and meta-analysis. Cancer Treat. Rev. *53*, 120–127.

Baselet, B., Azimzadeh, O., Erbeldinger, N., Bakshi, M.V., Dettmering, T., Janssen, A., Ktitareva, S., Lowe, D.J., Michaux, A., Quintens, R., et al. (2017). Differential impact of single-dose Fe ion and X-Ray irradiation on endothelial cell transcriptomic and proteomic responses. Front. Pharmacol. *8*, 570.

Beheshti, A., Ray, S., Fogle, H., Berrios, D., and Costes, S.V. (2018). A microRNA signature and TGF-beta1 response were identified as the key master regulators for spaceflight response. PLoS One *13*, e0199621.

Beheshti, A., Stevenson, K., Vanderburg, C., Ravi, D., McDonald, J.T., Christie, A.L., Shigemori, K., Jester, H., Weinstock, D.M., and Evens, A.M. (2019). Identification of circulating serum multi-MicroRNA signatures in human DLBCL models. Sci. Rep. *9*, 17161.

Boerma, M., Nelson, G.A., Sridharan, V., Mao, X.W., Koturbash, I., and Hauer-Jensen, M. (2015). Space radiation and cardiovascular disease risk. World J. Cardiol. *7*, 882–888.

Chen, J.Q., Papp, G., Szodoray, P., and Zeher, M. (2016). The role of microRNAs in the pathogenesis of autoimmune diseases. Autoimmun. Rev. *15*, 1171–1180.

Clarencon, D., Lestaevel, P., Laval, J.D., Multon, E., Gourmelon, P., Buguet, A., and Cespuglio, R. (1999). Voltammetric measurement of blood nitric oxide in irradiated rats. Int. J. Radiat. Biol. *75*, 201–208.

Colpaert, R.M.W., and Calore, M. (2019). MicroRNAs in cardiac diseases. Cells *8*, 737.

Condorelli, G., Latronico, M.V., and Dorn, G.W., 2nd (2010). microRNAs in heart disease: putative novel therapeutic targets? Eur. Heart J. *31*, 649–658.

Cucinotta, F.A., Hamada, N., and Little, M.P. (2016). No evidence for an increase in circulatory disease mortality in astronauts following space radiation exposures. Life Sci. Space Res. (Amst.) *10*, 53–56.

Cucinotta, F.A., To, K., and Cacao, E. (2017). Predictions of space radiation fatality risk for exploration missions. Life Sci. Space Res. (Amst.) *13*, 1–11.

Delp, M.D., Charvat, J.M., Limoli, C.L., Globus, R.K., and Ghosh, P. (2016). Apollo lunar astronauts show higher cardiovascular disease mortality: possible deep space radiation effects on the vascular endothelium. Sci. Rep. *6*, 29901.

Durante, M., and Cucinotta, F.A. (2011). Physical basis of radiation protection in space travel. Mod. Phys. *83*, 1245–1281.

Eyileten, C., Wicik, Z., De Rosa, S., Mirowska-Guzel, D., Soplinska, A., Indolfi, C., Jastrzebska-Kurkowska, I., Czlonkowska, A., and Postula, M. (2018). MicroRNAs as diagnostic and prognostic biomarkers in ischemic stroke-A comprehensive review and bioinformatic analysis. Cells *7*, 249.

Girdhani, S., Lamont, C., Hahnfeldt, P., Abdollahi, A., and Hlatky, L. (2012). Proton irradiation suppresses angiogenic genes and impairs cell invasion and tumor growth. Radiat. Res. *178*, 33–45.

Girdhani, S., Sachs, R., and Hlatky, L. (2013). Biological effects of proton radiation: what we know and don't know. Radiat. Res. *179*, 257–272.

Goligorsky, M.S. (2010). Microvascular rarefaction: the decline and fall of blood vessels. Organogenesis *6*, 1–10.

Grabham, P., Hu, B.R., Sharma, P., and Geard, C. (2011). Effects of ionizing radiation on three-dimensional human vessel models: differential effects according to radiation quality and cellular development. Radiat. Res. *175*, 21–28.

Grabham, P., and Sharma, P. (2013). The effects of radiation on angiogenesis. Vasc. Cell *5*, 19.

Grabham, P., Sharma, P., Bigelow, A., and Geard, C. (2013). Two distinct types of the inhibition of vasculogenesis by different species of charged particles. Vasc. Cell *5*, 16.

Grabham, P.W., Bigelow, A., and Geard, C. (2012). Effects of ionizing radiation on DNA repair dynamics in 3-Dimensional human vessel models: differential effects according to radiation quality. Int. J. Radiat. Biol. *6*, 493–500.

Hellweg, C.E., Baumstark-Khan, C., Schmitz, C., Lau, P., Meier, M.M., Testard, I., Berger, T., and Reitz, G. (2011). Activation of the nuclear factor kappaB pathway by heavy ion beams of different linear energy transfer. Int. J. Radiat. Biol. *87*, 954–963.

Hromadnikova, I., Kotlabova, K., Hympanova, L., and Krofta, L. (2015). Cardiovascular and cerebrovascular disease associated microRNAs are dysregulated in placental tissues affected with gestational hypertension, preeclampsia and intrauterine growth restriction. PLoS One *10*, e0138383.

Hughes-Fulford, M., Chang, T.T., Martinez, E.M., and Li, C.F. (2015). Spaceflight alters expression of microRNA during T-cell activation. FASEB J. *29*, 4893–4900.

Hughson, R.L., Helm, A., and Durante, M. (2018). Heart in space: effect of the extraterrestrial environment on the cardiovascular system. Nat. Rev. Cardiol. *15*, 167–180.

Ianzini, F., Kosmacek, E.A., Nelson, E.S., Napoli, E., Erenpreisa, J., Kalejs, M., and Mackey, M.A. (2009). Activation of meiosis-specific genes is associated with depolyploidization of human tumor cells following radiation-induced mitotic catastrophe. Cancer Res. *69*, 2296–2304.

Konovalova, J., Gerasymchuk, D., Parkkinen, I., Chmielarz, P., and Domanskyi, A. (2019). Interplay between MicroRNAs and oxidative stress in neurodegenerative diseases. Int. J. Mol. Sci. *20*, 6055.

Krutzfeldt, J., Rajewsky, N., Braich, R., Rajeev, K.G., Tuschl, T., Manoharan, M., and Stoffel, M. (2005). Silencing of microRNAs in vivo with 'antagomirs'. Nature *438*, 685–689.

Kuosmanen, S.M., Hartikainen, J., Hippelainen, M., Kokki, H., Levonen, A.L., and Tavi, P. (2015). MicroRNA profiling of pericardial fluid samples from patients with heart failure. PLoS One *10*, e0119646.

Macfarlane, L.A., and Murphy, P.R. (2010). MicroRNA: biogenesis, function and role in cancer. Curr. Genomics *11*, 537–561.

Malkani, S., Cekanaviciute, E., Mortreux, M., Okunola, H., Tarbier, M., Schreurs, A.S., Shirazi-Fard, Y., Tahimic, C.G.T., Cheng-Campbell, M., Blaber, E.A., et al. (2020). Circulating miRNA signature predicts and rescues spaceflight associated health risks (July 2020). https://doi.org/10.2139/ssrn.3641936.

Mao, X.W., Boerma, M., Rodriguez, D., Campbell-Beachler, M., Jones, T., Stanbouly, S., Sridharan, V., Wroe, A., and Nelson, G.A. (2018). Acute effect of low-dose space radiation on mouse retina and retinal endothelial cells. Radiat. Res. *190*, 45–52.

Mao, X.W., Favre, C.J., Fike, J.R., Kubinova, L., Anderson, E., Campbell-Beachler, M., Jones, T., Smith, A., Rightnar, S., and Nelson, G.A. (2010). High-LET radiation-induced response of microvessels in the Hippocampus. Radiat. Res. *173*, 486–493.

Mitchell, A., Pimenta, D., Gill, J., Ahmad, H., and Bogle, R. (2019). Cardiovascular effects of space radiation: implications for future human deep space exploration. Eur. J. Prev. Cardiol. *26*, 1707–1714.

Moslehi, J.J. (2016). Cardiovascular toxic effects of targeted cancer therapies. N. Engl. J. Med. *375*, 1457–1467.

Neves, K.B., Rios, F.J., van der Mey, L., Alves-Lopes, R., Cameron, A.C., Volpe, M., Montezano, A.C., Savoia, C., and Touyz, R.M. (2018). VEGFR (vascular endothelial growth factor receptor) inhibition induces cardiovascular damage via redox-sensitive processes. Hypertension *71*, 638–647.

Patel-Hett, S., and D'Amore, P.A. (2011). Signal transduction in vasculogenesis and developmental angiogenesis. Int. J. Dev. Biol. *55*, 353–363.

Paul, A.M., Cheng-Campbell, M., Blaber, E.A., Anand, S., Bhattacharya, S., Zwart, S.R., Crucian, B.E., Smith, S.M., Meller, R., Grabham, P., et al. (2020). Beyond low-earth orbit: characterizing the immune profile following simulated spaceflight conditions for deep space missions. iScience In press.

Scheuring, R.A., Mathers, C.H., Jones, J.A., and Wear, M.L. (2009). Musculoskeletal injuries and minor trauma in space: incidence and injury mechanisms in U.S. astronauts. Aviat. Space Environ. Med. *80*, 117–124.

Sharma, P., Templin, T., and Grabham, P. (2013). Short term effects of gamma radiation on endothelial barrier function: uncoupling of PECAM-1. Microvasc. Res. *86*, 11–20.

Simone, N.L., Soule, B.P., Ly, D., Saleh, A.D., Savage, J.E., Degraff, W., Cook, J., Harris, C.C., Gius, D., and Mitchell, J.B. (2009). Ionizing radiation-induced oxidative stress alters miRNA expression. PLoS One *4*, e6377.

Simonsen, L.C., Slaba, T.C., Guida, P., and Rusek, A. (2020). NASA's first ground-based Galactic Cosmic Ray Simulator: enabling a new era in space radiobiology research. PLoS Biol. *18*, e3000669.

Sofia Vala, I., Martins, L.R., Imaizumi, N., Nunes, R.J., Rino, J., Kuonen, F., Carvalho, L.M., Ruegg, C., Grillo, I.M., Barata, J.T., et al. (2010). Low doses of ionizing radiation promote tumor growth and metastasis by enhancing angiogenesis. PLoS One *5*, e11222.

Soucy, K.G., Lim, H.K., Kim, J.H., Oh, Y., Attarzadeh, D.O., Sevinc, B., Kuo, M.M., Shoukas, A.A., Vazquez, M.E., and Berkowitz, D.E. (2011). HZE (5)(6)Fe-ion irradiation induces endothelial dysfunction in rat aorta: role of xanthine oxidase. Radiat. Res. *176*, 474–485.

Suman, S., Kumar, S., Moon, B.H., Strawn, S.J., Thakor, H., Fan, Z., Shay, J.W., Fornace, A.J., Jr., and Datta, K. (2016). Relative biological effectiveness of energetic heavy ions for intestinal tumorigenesis shows male preponderance and radiation type and energy dependence in APC(1638N/+) mice. Int. J. Radiat. Oncol. Biol. Phys. *95*, 131–138.

Templin, T., Young, E.F., and Smilenov, L.B. (2012). Proton radiation-induced miRNA signatures in mouse blood: characterization and comparison with 56Fe-ion and gamma radiation. Int. J. Radiat. Biol. *88*, 531–539.

Vanderburg, C., and Beheshti, A. (2020b). MicroRNAs (miRNAs), the Final Frontier: The Hidden Master Regulators Impacting Biological Response in All Organisms Due to Spaceflight (THREE).

Wild-Bode, C., Weller, M., Rimner, A., Dichgans, J., and Wick, W. (2001). Sublethal irradiation promotes migration and invasiveness of glioma cells: implications for radiotherapy of human glioblastoma. Cancer Res. *61*, 2744–2750.

Willey, C.D., Xiao, D., Tu, T., Kim, K.W., Moretti, L., Niermann, K.J., Tawtawy, M.N., Quarles, C.C., and Lu, B. (2010). Enzastaurin (LY317615), a protein kinase C beta selective inhibitor, enhances antiangiogenic effect of radiation. Int. J. Radiat. Oncol. Biol. Phys. *77*, 1518–1526.

Yu, T., Parks, B.W., Yu, S., Srivastava, R., Gupta, K., Wu, X., Khaled, S., Chang, P.Y., Kabarowski, J.H., and Kucik, D.F. (2011). Iron-ion radiation accelerates atherosclerosis in apolipoprotein E-deficient mice. Radiat. Res. *175*, 766–773.

Zhang, Y., Lu, T., Wong, M., Wang, X., Stodieck, L., Karouia, F., Story, M., and Wu, H. (2016). Transient gene and microRNA expression profile changes of confluent human fibroblast cells in spaceflight. FASEB J. *30*, 2211–2224.

Ziche, M., and Morbidelli, L. (2000). Nitric oxide and angiogenesis. J. Neurooncol. *50*, 139–148.

iScience, Volume *23*

Supplemental Information

LET-Dependent Low Dose and Synergistic Inhibition of Human Angiogenesis by Charged Particles: Validation of miRNAs that Drive Inhibition

Yen-Ruh Wuu, Burong Hu, Hazeem Okunola, Amber M. Paul, Elizabeth A. Blaber, Margareth Cheng-Campbell, Afshin Beheshti, and Peter Grabham

SUPPLEMENTAL INFORMATION

Supplemental Figure.

Supplemental Figure S1. Effect of antagomirs on micro-vessels grown in nutrient depleted media. (related to Figure 7). HUVECs were seeded into gel matrices and cultured in normal microvessel growth media with only 50% of the nutrient and growth factor additives. Single antagomirs and combinations of antagomirs were added to the media on days 0, 1, and 2. After 7 days the micro-vessels were fixed and the lengths determined as for irradiation experiments. All antagomirs to each miRNA promoted the growth of micro-vessels over the control cultures. Error bars are sems. Control is significantly different from all antagomirs and combinations (P= 0.0006). **(related to Figure 7).**

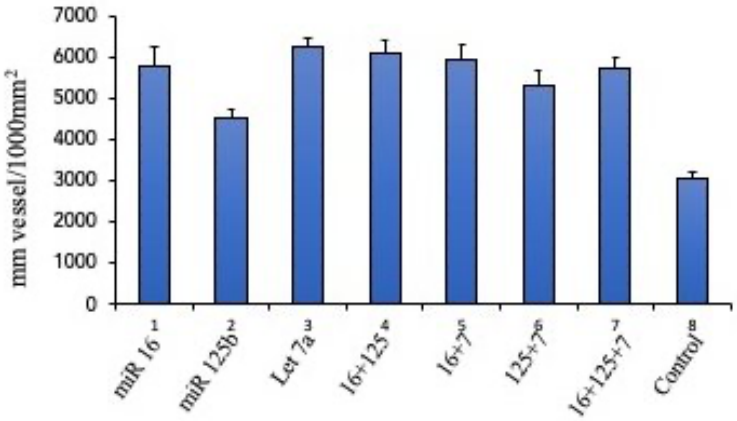

Transparent Methods

Ethics statement

All in vitro experiments were carried out on Human commercially available Human endothelial Cells. All animal experiments were approved by Brookhaven National Laboratory's (BNL)

Institutional Animal Care and Use Committee (IACUC) (protocol number: 506) and all experiment were performed by trained personnel in AAALAC accredited animal facilities at BNL, while conforming to the U.S. National Institutes of Health Guide for the Care and Use of Laboratory Animals.

Experimental design

Irradiations

Irradiation of micro-vessel models and animals were conducted at the NASA Space Radiation Laboratory (NSRL) at Brookhaven National Laboratory (BNL, Upton, NY). Samples were positioned in the plateau region of the Bragg curve and irradiated at room temperature. Dosimetry was performed by the NSRL physics staff.

Micro-vessel models, cultures were seeded at Columbia University in New York City then transported to BNL the same day. Irradiations were carried out the following day (Day 1) at NSRL. A 20 x 20cm beam was utilized. Since the heavy-ion beam at NSRL is horizontal, flasks containing 5 ml of medium were upended to a vertical position for a few minutes during irradiation. All cultures were irradiated with either individual ions or 0.5Gy of simGCRsim, all with sham irradiated controls. Sham controls were treated the same as irradiated micro-vessels (25 minutes outside the incubator). Micro-vessel cultures were transported back to Columbia University for further culture. Antagomirs (AUM biotech) were added to cultures 24hours and 48 hours after irradiations. All three antagomirs were added to cultures collectively at a of concentration of 0.5mm. Fixation was carried out with 4% paraformaldehyde 6 days after irradiations).

Mice, 15-week +/- 3-day old, *C57Bl/6J* wildtype (*Wt*) female mice were purchased from Jackson Laboratories and housed at Brookhaven National Laboratory (BNL, Upton, NY). Upon arrival to BNL, mice were quarantined and acclimated to a standard 12:12h light:dark cycle, with controlled

temperature/humidity for 1-week prior to cage acclimation. Food and water were given *ad libitum*, and standard bedding was changed once per week. Mice were cage acclimated (n=10 mice per group; 2 mice per cage to maintain social interaction).

On day 13, mice were transported on BNL base to the NASA Space Radiation Laboratory (NSRL) facility by animal care staff and were transferred to individual boxes. The following doses of irradiation were administered; simplified GCR sim (0.5 Gy), Gamma (5 Gy), and Sham control (0 Gy). For all animal irradiations a 60 cm x 60 cm beam was utilized for 50cGy simGCRsim. Sham controls were treated similar to GCR irradiated mice, including beam line (without irradiation) for the same duration as GCR simualtion, i.e. 25 minutes. For radiation dose equivalence and biological reference, we used 5 Gy gamma irradiation with the cesium resource available at BNL. Blood and tissues were collected at 24-hours post-irradiation and post-euthanasia by CO_2 overdose, followed by cervical dislocation. Blood was collected via the abdominal aorta in EDTA-coated tubes (0.5 M) and plasma was separated by centrifugation at 2,000xg for 15 minutes. Plasma was collected and flash frozen in liquid nitrogen for -80°C storage. A 100 µl aliquot of cellular fraction was flash frozen and stored at -80°C for RNA analyses, while the remaining cellular fraction was lysed with 1x RBC lysis buffer (Thermo Fisher Scientific) followed by flow cytometric preparation and analyses, as describe below. The heart was flash frozen and collected at the time of dissection. All tissues were stored at -80°C. Body weight tracking was performed on days 0, 7 and 14 days post irradiation.

Simulated GCR

To simulate GCR, we used the simplified GCR simulation of ions, energy, and doses determined by a NASA consensus formula that consists of 5 ions: protons at 1000 MeV, ^{28}Si at 600 MeV/n, ^{4}He at 250 MeV/n, ^{16}O at 350 MeV/n, ^{56}Fe at 600 MeV/n, and protons at 250 MeV, in the following

proportions; Protons 100MeV at 34.8%, Si at 1.1%, He at 18%, O at 5.8%, ^{56}Fe at 1%, and Protons 250 MeV at 39.3%. This mixture is the simplified version of the full GCR simulation and represents the proportions of ions found in space and thus translates to exploratory class missions (Simonsen et al 2020). The low LET particles (Protons and Helium) make up the majority of radiation although high LET ions generally have a greater RBE.

miRNA isolation, sequencing, and data analyses

Library construction and sequencing was performed from miRNAs isolated from plasma from the mouse experiments described above. The miRNA extraction was carried out using the QIAgen miRNeasy kit (#217004). The total RNA quality and quantity were analyzed using a Bioanalyzer 2100 (Agilent, CA, USA) with RIN number > 7. Approximately 1 μg of total RNA was used to prepare small RNA library according to protocol of TruSeq Small RNA Sample Prep Kits (Illumina, San Diego, USA). Single-end sequencing was performed using 50 bp on an Illumina Hiseq 2500 at the LC Sciences (Hangzhou, China) following the vendor's recommended protocol. The miRNA-seq raw fastq files can be found on NASA's GeneLab data repository/platform (https://genelab.nasa.gov/) with the following identifiers: for heart tissues, GLDS-334, DOI: 10.26030/cg2g-as49; and for plasma, GLDS-336, DOI: 10.26030/qasa-rr29.

Raw reads were subjected to an in-house software program, ACGT101-miR (LC Sciences, Houston, Texas, USA) to remove adapter dimers, junk, low complexity, common RNA families (rRNA, tRNA, snRNA, snoRNA) and repeats. Subsequently, unique sequences with length in 18~26 nucleotide were mapped to specific species precursors in miRBase 22.0 by BLAST search to identify known miRNAs and novel 3p- and 5p- derived miRNAs. Length variation at both 3' and 5' ends and one mismatch inside of the sequence were allowed in the alignment. The unique sequences mapping to specific species mature miRNAs in hairpin arms were identified as known

miRNAs. The unique sequences mapping to the other arm of known specific species precursor hairpin opposite to the annotated mature miRNA-containing arm were considered to be novel 5p- or 3p- derived miRNA candidates. The remaining sequences were mapped to other selected species precursors (with the exclusion of specific species) in miRBase 22.0 by BLAST search, and the mapped pre-miRNAs were further BLASTed against the specific species genomes to determine their genomic locations. The above two we defined as known miRNAs. The unmapped sequences were BLASTed against the specific genomes, and the hairpin RNA structures containing sequences were predicated from the flank 80 nt sequences using RNAfold software (http://rna.tbi.univie.ac.at/cgi-bin/RNAWebSuite/RNAfold.cgi). The criteria for secondary structure prediction were: (1) number of nucleotides in one bulge in stem (≤12); (2) number of base pairs in the stem region of the predicted hairpin (≥16); (3) cutoff of free energy (kCal/mol ≤-15); (4) length of hairpin (up and down stems + terminal loop ≥50); (5) length of hairpin loop (≤20); (6) number of nucleotides in one bulge in mature region (≤8); (7) number of biased errors in one bulge in mature region (≤4); (8) number of biased bulges in mature region (≤2); (9) number of errors in mature region (≤7); (10) number of base pairs in the mature region of the predicted hairpin (≥12); and (11) percent of mature in stem (≥80). Differential expression of miRNAs based on normalized deep-sequencing counts was analyzed by selectively using Fisher exact test, Chi-squared 2X2 test, Chi-squared nXn test, Student t test, or ANOVA based on the experimental design. The significance threshold was set to be 0.01 and 0.05 in each test.

To determine gene ontology (GO) and C2 pathways being regulated by the miRNAs we performed miRNA gene set analysis utilizing the RBiomirGS v0.2.12 R package (Zhang and Storey, 2018) from the processed miRNA analysis for all conditions in the plasma and heart

tissues. From the pathways we chose an FDR < 0.25 cutoff for significantly regulated pathways. We plotted the specific pathways with R packages ggplot2.

Cell culture

Prior to culturing 3D micro-vessels HUVEC (Lonza Inc, Allendale, NJ, USA) were cultured as 2D monolayers in complete endothelial basal medium (EBM; Lonza Inc., Allendale, NJ, USA), containing EGM medium (serum free) supplemented with 2% fetal bovine serum (FBS), human epidermal growth factor, hydrocortisone and bovine brain extract. Cells were kept in a humidified incubator (5% CO_2, 95% air), and the medium was changed twice a week. All cells used for experiments were cells thawed from a fresh vial.

3D HUVEC vessel model

In this study, 3D cell culture was performed according to the method initially described by (Davis and Camarillo, 1996) with modifications described in (Grabham et al., 2013). Briefly, Collagen gel solution (Rat tail Collagen Type 1 BD Biosciences, Bedford MA) was prepared on ice by mixing together the following stock solutions: 0.35% collagen solution, 10× M199 medium, and 1 M HEPES (pH 7.4) in a ratio of 8:1:1 by (volume). This solution was then mixed with matrigel (BD Biosciences, Bedford, MA) in a ratio of 3:1 by (volume). HUVEC grown in EGM on 2D cell culture dishes (80–90% confluence) were detached with a trypsin solution (0.025%). and resuspended in EGM2 (Lonza Inc, Allendale, NJ, USA). The cell solution was mixed with the gel solution in a ratio 1:5 (by volume). The resulting cell suspension contained a final cell suspension of 1×10^6 cells/ml. 25 µl was dropped onto the cell growing surface inside a tissue culture flask (T25) (Corning) and allowed to gel at 37 °C for 30 min. The gel matrices were then overlaid with EGM-2 medium for 7 days with daily media changes. EBM-2 consists of EGM-2 media supplemented with 2% FBS human fibroblast growth factor B (hFGF-B), human epidermal

growth factor (hEGF), human vascular endothelial cell growth factor (hVEGF), long R insulin-like growth factor 1 (R3-IGF-1), ascorbic acid, hydrocortisone and heparin. 50 nM Phorbol 12-Myristate 13-acetate (PMA) (Millipore Sigma) was also added to the growth media. Cells embedded in 200–300 μm thick gel matrices were incubated at 37 °C in a humidified incubator (5% CO_2, 95% air) for the times indicated. The medium was refreshed every 24 h or as otherwise stated in individual experiments.

Immunocytochemistry, Imaging, and microvessel analysis

All micro-vessel cultures were fixed and stained as for monolayers. Fixed in 4% paraformaldehyde followed by three washes in Phosphate buffered saline (PBS) with 0.5% Triton-X, and finally in PBS. 5-(4,6-Dichlorotriazinyl) Aminofluorescein (DTAF) (Thermofisher Scientific) was used to as a fluorescent green stain for all proteins to visualize micro-vessels. LIVE/DEAD™ Fixable Red Dead Cell Stain (Thermo-Fisher Scientific) was used to as a fluorescent red stain to visualize micro-vessels. Anti Collagen polyclonal antibody (Abcam) followed by AlexaFluor 488 Goat anti-Rabbit IgG (H+L) (Thermo-Fisher) was used to visualizer collagen tunnels and Anti Tubulin Ab-6 (Clone TBN06) monoclonal antibody (Thermo-Fisher) followed by AlexaFluor 488 Goat anti-Mouse IgG (H+L) (ThermoFisher) to detect bundled microtubules.

Images were captured on a Nikon TE 200 confocal C1 microscope with EZ-C1 software. Analysis of images was carried out using NIH Image J v. 1.44k software (Schneider et al., 2012). Initial analysis (Figures 2 and 3) was carried out on randomly selected 20X fields from within the gel matrix. Thresholded images of micro-vessels were outlined as perimeters then divided by 2 for length measurements. For the improved analysis (Figures 3 and 4) the field size was increased 4-fold by using images captured by a 10X objective. The mature micro-vessels were defined more rigorously as those of a minimum diameter of 12.5 μm. This step eliminated many immature thin

vessels (especially in the heavy ion treated samples) and reduced the effective doses. Finally, the sample fields were standardized, by imaging micro-vessels at a constant depth (50 □m above the substrate). All analyses were carried out blind.

Statistical Analysis

For micro-vessel models differences between means were analyzed with the data-analysis add-in of Microsoft Excel using Student's *t*-test assuming unequal variances among groups. *p*-values below 0.05 were considered statistically significant.

STARZ METHODS

KEY RESOURCE TABLE

REAGENT or RESOURCE	SOURCE	IDENTIFIER
Antibodies		
Rat Anti-Collagen I Polyclonal Antibody	Abcam	ab254113
Anti Tubulin Ab-6 (Clone TBN06)	Thermofisher Scientific	MS-1226-PO
Experimental Models: Cell Lines		
Human Umbilical Vein Endothelial Cells: HUVEC	Lonza	CC-2519
Chemicals, Peptides, and Recombinant Proteins		
EGM-2 Endothelial Cell Growth Medium-2 Bullet-Kit	Lonza	CC-3162
EGM Endothelial Cell Growth Medium Bullet-Kit	Lonza	CC-3124
Rat tail Collagen Type 1	BD Biosciences	354236
Matrigel Matrix	BD Biosciences	356230
Porbol-12-myristate-13-acetate: PMA	Millipore	524400
5-(4,6-Dichlorotriazinyl) Aminofluorescein (DTAF)	Thermofisher Scientific	D 16
Fixable Red Dead Cell Stain	Thermofisher Scientific	L 23102

AlexaFluor 488 Goat anti-Rabbit IgG (H+L)	Thermofisher Scientific	R37116
AlexaFluor 488 Goat anti-IgG (H+L)	Thermofisher Scientific	R37120
MP Biomedicals™ Trypsin-EDTA Solution	Thermofisher Scientific	ICN1689149
Antagomirs	AUM Biotech	
AUM-ANT-B AUM-ANT-B AUM-ANT-B AUM-ANT-B AUM-ANT-B AUM-ANT-B AUM-ANT-B AUM-ANT-B AUM-ANT-B AUM-ANT-B AUM-ANT-B AUM-ANT-B AUM-SCR-B		hsa-mir-16-5p_1 hsa-mir-16-5p_2 hsa-mir-16-5p_3_BLK hsa-mir-16-5p_4_BLK hsa-miR-125b-5p_1 hsa-miR-125b-5p_2 hsa-miR-125b-5p_3_BLK hsa-miR-125b-5p_4_BLK hsa-let-7a-5p_1 hsa-let-7a-5p_2 **hsa-let-7a-5p_3_BLK** **hsa-let-7a-5p_4_BLK** **Scramble Control**
Biological Samples		
Mouse Heart	*C57Bl/6J Wt* female	n/a
Mouse Plasma	*C57Bl/6J Wt* female	n/a
Critical Commercial Assays		
miRNeasy Mini Kit	QIAgen	217004
miRNeasy serum/plasma kit	QIAgen	217184
TruSeq Small RNA Sample Prep Kits	Illumina	RS-200-0012
Experimental Models: Organisms/Strains		
C57Bl/6J Wt female mice	Jackson Laboratories	000664
Simplified 5-ion GCR Siulation	Protons at 1000 MeV, ^{28}Si at 600 MeV/n, ^{4}He at 250 MeV/n, ^{16}O at 350	n/a

	MeV/n, ^{56}Fe at 600 MeV/n, and protons at 250 MeV	
Software and Algorithms		
ACGT101-miR (LC Sciences)	n/a	n/a
miRBase 22.0	(Kozomara et al., 2019)	http://www.mirbase.org/
RNAfold software	n/a	http://rna.tbi.univie.ac.at/cgi-bin/RNAWebSuite/RNAfold.cgi
RBiomirGS v0.2.12 R package	(Zhang and Storey, 2018)	https://github.com/jzhangc/git_RBiomirGS
R package v3.6.1		https://www.r-project.org/
ggplot2 v3.3.1	Wickham, 2016	https://ggplot2.tidyverse.org
Other		
Illumina Hiseq 2500	LC Sciences	n/a